[5] N. Yang, C. Caloz, and K. Wu, "Co-designed CPS UWB filter-antenna system," in *Proc. IEEE AP-S Int. Symp.*, Jun. 2007, pp. 1433–1436.
[6] T. L. Nadan, J. P. Coupez, S. Toutain, and C. Person, "Optimization and miniaturization of a filter/antenna multi-function module using a composite ceramic-foam substrate," in *IEEE MTT-S Int. Microw. Symp. Dig.*, Jun. 1999, pp. 219–222.
[7] A. Abbaspour-Tamijani, J. Rizk, and G. Rebeiz, "Integration of filters and microstrip antennas," in *Proc. IEEE AP-S Int. Symp.*, Jun. 2002, pp. 874–877.
[8] W. L. Stutzman and G. A. Thiele, *Antenna Theory and Design*. New York: Wiley, 1998.
[9] D. M. Pozar, *Microwave Engineering*, 3rd ed. New York: Wiley, 2005, ch. 8.
[10] M. Matsuo, H. Yabuki, and M. Makimoto, "The design of a half-wavelength resonator BPF with attenuation poles at desired frequencies," in *IEEE MTT-S Int. Microw. Symp. Dig.*, 2000, pp. 1181–1184.

Shaping Axis-Symmetric Dual-Reflector Antennas by Combining Conic Sections

Fernando J. S. Moreira and José R. Bergmann

***Abstract*—A simple procedure for the shaping of axis-symmetric dual-reflector antennas is described. The shaping procedure is based on the consecutive concatenation of local conic sections suited to provide, under geometrical optics (GO) principles, an aperture field with uniform phase, together with a prescribed amplitude distribution. The procedure has fast numerical convergence and is valid for any circularly symmetric dual-reflector configuration. To illustrate the procedure two representative configurations are investigated. The GO shaping results are validated using accurate method-of-moments analysis.**

***Index Terms*—Geometrical optics, reflector antennas, reflector shaping.**

I. Introduction

A procedure for the geometrical optics (GO) shaping of circularly symmetric Cassegrain and Gregorian antennas has been presented recently [1]. It is based on the combination of local dual-reflector systems to describe the generatrices of the sub- and main-reflectors, providing an aperture illumination with a uniform phase distribution together with a prescribed amplitude distribution. The procedure represents an improvement over traditional methods [2], [3] as no ordinary differential equation needs to be solved. The use of curved (biparabolic) surfaces to locally represent the reflectors together with ray tracing (i.e., GO concepts) had already been adopted in [4] to establish a nondifferential set of equations to shape offset dual-reflector antennas.

In [1] the authors adopted rectangular coordinates to describe the local conic sections representing the reflectors' generatrices, leading to a nonlinear algebraic equation, which was approximated to provide an one-step iterative solution. In the present work we improve the solution by using polar coordinates to represent the conic sections. That renders an one-step iterative procedure with simple linear algebraic equations, thus avoiding any approximation. Another interesting feature of the present formulation is that it is valid for any shaped axis-symmetric dual-reflector configuration based on the classical axis-displaced Cassegrain (ADC), Gregorian (ADG), ellipse (ADE), or hyperbola (ADH) [5].

Manuscript received March 25, 2010; revised July 07, 2010; accepted September 09, 2010. Date of publication December 30, 2010; date of current version March 02, 2011. This work was supported in part by the Brazilian agencies CNPq (INCT CSF), and CAPES under Grant RH-TVD-254/2008.

F. J. S. Moreira is with the Department of Electronics Engineering of the Federal University of Minas Gerais, 30161-970 Belo Horizonte, MG, Brazil (e-mail: fernandomoreira@ufmg.br).

J. R. Bergmann is with the Center for Telecommunications Studies of the Catholic University, 22453-900 Rio de Janeiro, RJ, Brazil.

Digital Object Identifier 10.1109/TAP.2010.2103028

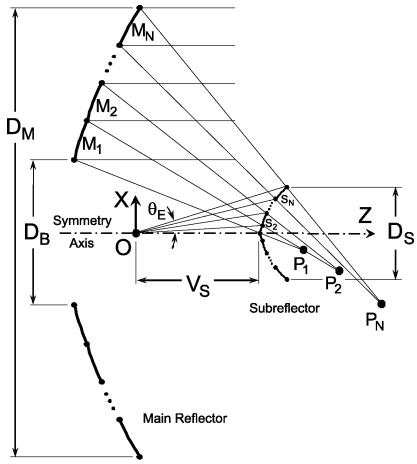

Fig. 1. Dual-reflector shaping by consecutively combining conic sections (ADC-like configuration).

In Section II the GO dual-reflector shaping formulation is presented assuming a shaped Cassegrain (or ADC) geometry. In Section III, the formulation is extended to other axis-symmetric dual-reflector configurations (ADG, ADE, and ADH). Then, the shaping of two representative dual-reflector antennas (ADC and ADE configurations) is conducted to illustrate the procedure. The convergence of the shaping procedure is investigated and compared to another procedure based on the numerical solution of an ordinary differential equation [3]. The radiation characteristics of the shaped dual-reflector antennas are numerically obtained by a method-of-moments (MoM) analysis in order to validate the applicability of the proposed shaping technique. The MoM software used in the present analysis has been successfully applied in previous reflector-antenna synthesis (e.g., [6]).

II. Formulation of the Shaping Procedure

The basic idea is to represent the reflector generatrices by conic sections consecutively concatenated, as depicted in Fig. 1. Notice that a shaped ADC configuration will be adopted to derive the formulation, but in Section III the procedure will be extended to the other axis-symmetric dual-reflector antennas [5], [7].

The conic sections describing the subreflector $(S_n, n = 1, \ldots, N)$ have two focci. One is always at the origin O (where the feed phase-center is assumed to be) and the other at point P_n. As n is varied from 1 to N, P_n spans the locus of the subreflector caustic. P_n is also the focus of the parabolic section M_n that describes a corresponding portion of the main reflector. The axis of M_n passes through P_n and is parallel to the symmetry axis of both reflectors (z axis), such that all the rays reflected at the main reflector arrive parallel to each other at the antenna aperture plane, thus providing a uniform phase distribution at the aperture, according to GO principles. Another GO principle used to define the conic sections is the energy conservation in the bundle of rays that departs from O and reflects at S_n and M_n before reaching the antenna aperture.

In order to uniquely define the conic sections S_n and M_n at each iteration n, four parameters must be determined: the focal distance F_n

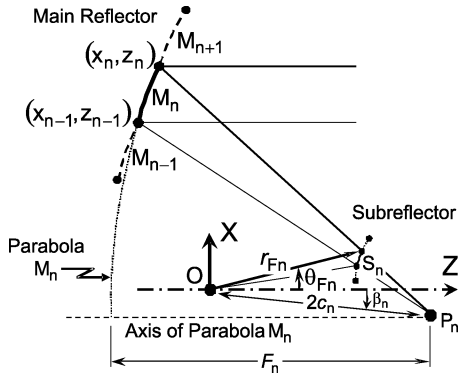

Fig. 2. Conic-section parameters.

of the parabolic section M_n, the interfocal distance $2c_n$ (i.e., the distance between O and P_n) and the eccentricity e_n of the subreflector conic section S_n, and the tilt angle β_n of the axis of S_n with respect to the z-axis (see Fig. 2). Consequently, four equations are needed to solve the problem at each step n. The iterative process marches on with θ_{Fn}, which is the feed ray direction (with respect to the z-axis) toward the superior extreme of S_n (see Fig. 2). θ_{Fn} is uniformly varied from $\theta_{F0} = 0$ to the subreflector edge at $\theta_{FN} = \theta_E$, such that $\Delta\theta_F = \theta_{Fn} - \theta_{Fn-1} = \theta_E/N$. In principle, the accuracy of the shaping procedure increases with N. The iterations start at $n = 0$ with $\theta_{F0} = 0$ and $r_{F0} = V_S$, where r_F is the distance from O to the subreflector along the ray-direction θ_F and V_S is the desired distance between the feed phase-center and the subreflector apex (see Fig. 1).

From the polar equation of S_n one obtains the following relation:

$$r_F(\theta_F) = \frac{a_n}{b_n \cos\theta_F + d_n \sin\theta_F - 1} \tag{1}$$

for $\theta_{Fn-1} \le \theta_F \le \theta_{Fn}$, where

$$a_n = c_n(e_n - 1/e_n), \tag{2}$$

$$b_n = e_n \cos\beta_n, \tag{3}$$

$$d_n = e_n \sin\beta_n. \tag{4}$$

Equation (1) is general and may represent an ellipse ($0 < e_n < 1$), a hyperbola ($|e_n| > 1$), or any other conic section. To ensure a uniform phase distribution at the antenna aperture, it is enforced a constant path length (ℓ_o) from O to the aperture plane (assumed at $z = 0$). The mapping relation between θ_F and the Cartesian coordinate x of the corresponding aperture point (which is also the x coordinate of the main reflector) is given by [8]

$$\frac{x}{\ell_o} = \frac{(2a_n/\ell_o) + 1 + b_n - d_n \cot(\theta_F/2)}{d_n + (b_n - 1)\cot(\theta_F/2)}. \tag{5}$$

The first shaping equation of the n-th step is obtained from the polar equations of S_n and M_n and establishes a relation between ℓ_o and the unknowns

$$\begin{aligned}\ell_o &= 2F_n + \frac{2c_n}{e_n} - 2c_n\cos\beta_n \\ &= 2F_n + \frac{2c_n}{e_n}(1 - b_n),\end{aligned} \tag{6}$$

where the constant path ℓ_o must be specified *a priori*. For design purposes, notice that ℓ_o is approximately twice the distance between sub and main reflectors. The second equation is obtained from (1)

$$r_{Fn-1} = \frac{a_n}{b_n \cos\theta_{Fn-1} + d_n \sin\theta_{Fn-1} - 1} \tag{7}$$

where θ_{Fn-1} and r_{Fn-1} are known from the previous step $(n-1)$. The third equation is obtained from (5)

$$\frac{x_{n-1}}{\ell_o} = \frac{(2a_n/\ell_o) + 1 + b_n - d_n \cot(\theta_{Fn-1}/2)}{d_n + (b_n - 1)\cot(\theta_{Fn-1}/2)} \tag{8}$$

where x_{n-1} is the main-reflector x coordinate obtained in the previous step $(n-1)$ (see Fig. 2).

The last equation is derived by applying the conservation of energy along the tube of rays that departs from O and arrives at the aperture plane after being reflected by S_n and M_n. The conservation of energy is described by the following integral:

$$\int_0^{\theta_{Fn}} G_F(\theta_F)\, r_F^2\, \sin\theta_F\, d\theta_F = N_F \int_{D_B/2}^{x_n} G_A(x)\, x\, dx \tag{9}$$

where $G_F(\theta_F)$ is the circularly-symmetric radiated feed power density, $G_A(x)$ is the desired circularly-symmetric power density at the antenna aperture, and

$$N_F = \frac{\int_0^{\theta_E} G_F(\theta_F)\, r_F^2\, \sin\theta_F\, d\theta_F}{\int_{D_B/2}^{D_M/2} G_A(x)\, x\, dx} \tag{10}$$

is a normalization factor that assures that all feed power intercepted by the subreflector is conserved at the antenna aperture. In (9) and (10) D_B is the projected diameter of the main-reflector opening and D_M is the projected main-reflector diameter (see Fig. 1). Both D_M and D_B are input parameters for the shaping procedure. In principle, $D_B > D_S$ to avoid the subreflector blockage of the main-reflector reflected rays and also to allow feed access to the principal focus (O) of the dual-reflector system (see Fig. 1). Observe that, for $n = 0$, $x_n = D_B/2$. After x_n is numerically calculated from (9), the forth equation is obtained from (5) with $\theta_F = \theta_{Fn}$

$$\frac{x_n}{\ell_o} = \frac{(2a_n/\ell_o) + 1 + b_n - d_n \cot(\theta_{Fn}/2)}{d_n + (b_n - 1)\cot(\theta_{Fn}/2)} \tag{11}$$

which, together with (6)–(8), is used to determine the conic parameters F_n, $2c_n$, e_n, and β_n.

A. Linear System Solution

Substituting (6) and (7) into (8) and (11), one obtains the following linear system:

$$f_1 b_n + g_1 d_n = h_1 \tag{12}$$

$$f_2 b_n + g_2 d_n = h_2 \tag{13}$$

where

$$f_1 = x_{n-1}\cot(\theta_{Fn-1}/2) - \ell_o - 2r_{Fn-1}\cos\theta_{Fn-1} \tag{14}$$

$$f_2 = x_n \cot(\theta_{Fn}/2) - \ell_o - 2r_{Fn-1}\cos\theta_{Fn-1} \tag{15}$$

$$g_1 = x_{n-1} + \ell_o \cot(\theta_{Fn-1}/2) - 2r_{Fn-1}\sin\theta_{Fn-1} \tag{16}$$

$$g_2 = x_n + \ell_o \cot(\theta_{Fn}/2) - 2r_{Fn-1}\sin\theta_{Fn-1} \tag{17}$$

$$h_1 = x_{n-1}\cot(\theta_{Fn-1}/2) + \ell_o - 2r_{Fn-1} \tag{18}$$

$$h_2 = x_n \cot(\theta_{Fn}/2) + \ell_o - 2r_{Fn-1}. \tag{19}$$

The solutions of (12) and (13) are

$$b_n = \frac{h_1 g_2 - h_2 g_1}{f_1 g_2 - f_2 g_1} \tag{20}$$

$$d_n = \frac{f_1 h_2 - f_2 h_1}{f_1 g_2 - f_2 g_1}. \tag{21}$$

The conic parameters are then calculated as follows. Equations (20) and (21) are substituted into (3) and (4) in order to obtain e_n and β_n. Then, (20) and (21) are substituted into (7) to obtain a_n. Once e_n and a_n are known, $2c_n$ is obtained from (2). Finally, F_n is calculated from (6).

With the conic parameters determined, the subreflector point at $\theta_F = \theta_{Fn}$ is located by the vector

$$r_{Fn} \cos\theta_{Fn}\ \hat{z} + r_{Fn} \sin\theta_{Fn}\ \hat{x} \tag{22}$$

where r_{Fn} is given by (1) at $\theta_F = \theta_{Fn}$. The corresponding main-reflector point is located by the vector

$$z_n \hat{z} + x_n \hat{x} \tag{23}$$

where the Cartesian coordinate z_n is given by the parabolic equation of M_n

$$z_n = \frac{(x_n - 2c_n \sin\beta_n)^2}{4F_n} - F_n + 2c_n \cos\beta_n. \tag{24}$$

Finally, the location of P_n at the subreflector caustic is given by the vector

$$2c_n \cos\beta_n\ \hat{z} + 2c_n \sin\beta_n\ \hat{x}. \tag{25}$$

The steps are repeated until $\theta_{FN} = \theta_E$ (i.e., $n = N$).

Once $n+1$ points are obtained for each reflector, their generatrices may be described by any standard interpolation procedure, depending on the reflector-antenna analysis method adopted. However, one should notice that the sub and main reflectors described by the conic sections are continuous and have continuous first derivatives, as two consecutive local conic sections share the same optical path (from O to the main-reflector aperture) at their common point, which means that Snell's law is satisfied at that point.

III. Other Axis-Symmetric Dual-Reflector Configurations

The formulation derived in Section II assumed a shaped Cassegrain (or ADC) antenna, as illustrated in Figs. 1 and 2. However, the shaping procedure can be extended to other dual-reflector configurations [5], [7]. For a shaped Gregorian (or ADG) antenna, as illustrated in Fig. 3(a), one just needs to change the sign of x_n after its calculation from (9). For a shaped ADE, depicted in Fig. 3(b), the feed illumination toward the antenna aperture is reversed. In this case, for the calculation of x_n one must replace (9) by

$$\int_0^{\theta_{Fn}} G_F(\theta_F)\ r_F^2\ \sin\theta_F\ d\theta_F = N_F \int_{x_n}^{D_M/2} G_A(x)\ x\ dx \tag{26}$$

where, for $n = 0$, $x_n = D_M/2$. Finally, for a shaped ADH antenna, illustrated in Fig. 3(c), one must use (26) to calculate x_n, changing its sign afterward.

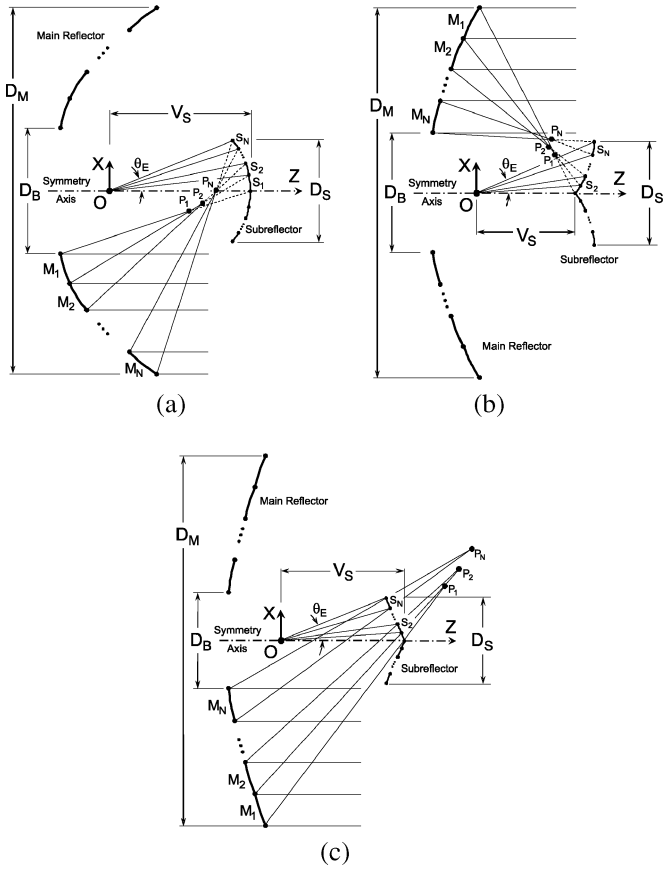

Fig. 3. Other shaped axis-symmetric dual-reflector antennas based on the (a) ADG, (b) ADE, and (c) ADH configurations.

IV. Results

In oder to illustrate the shaping procedure, an ADC and an ADE antennas are synthesized. As the synthesis is based on GO principles, the radiation patterns are analyzed by the method of moments (MoM) for bodies of revolution [9].

A. Shaped ADC Antenna

The first geometry is the Cassegrain configuration presented in [1], where the dimensions of the shaped antenna were specified with the help of a classical ADC with the following dimensions: $D_M = 6$ m, $D_B = D_S = 0.6$ m, $\ell_o = 3$ m, and $\theta_E = 30^\circ$. From [5] one obtains $V_S = 0.409$ m. The operating frequency is 5 GHz, such that $D_M \approx 100\ \lambda$. The sub- and main-reflector generatrices of the classical ADC are illustrated with dotted lines in Fig. 4. Applying the procedure of Section II, both reflectors are shaped to provide a uniform amplitude distribution over the illuminated portion of the aperture (i.e., $G_A(x)$ is constant from $x_0 = D_B/2$ to $x_N = D_M/2$, being null elsewhere). The feed model is the same adopted in [1]

$$G_F(\theta_F) = \frac{\cos^{2p}(\theta_F/2)}{r_F^2} \tag{27}$$

with $p = 83$ to provide -25 dB edge taper [1]. The shaped reflectors' generatrices are plotted with solid lines in Fig. 4 together with the shaped subreflector caustic. The maximum deviation of the shaped reflectors with respect to the classical configuration is approximately 7 cm for the subreflector and 4 cm for the main reflector (see Fig. 4). Both

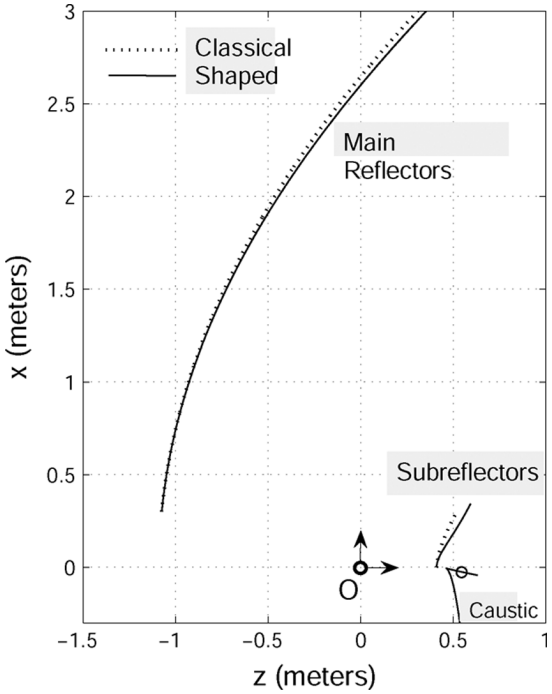

Fig. 4. Sub- and main-reflector generatrices of the classical (dotted lines) and shaped (solid lines) ADC antennas. The caustic refers to the shaped subreflector.

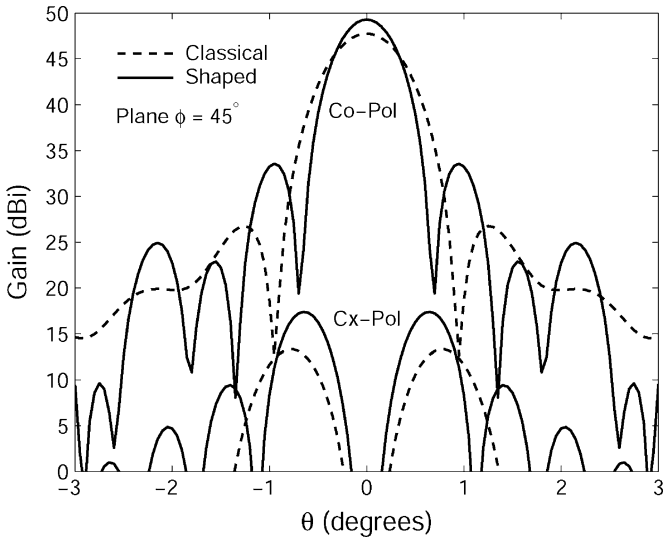

Fig. 5. Diagonal-plane radiation patterns of the classical (dashed lines) and shaped (solid lines) ADC antennas at 5 GHz. Reflectors shaped with $\Delta\theta_F \approx 10^{-4} \times \theta_E$.

classical and shaped antennas, fed by the linearly polarized feed model of (27), were analyzed by the MoM technique (the central hole of the main reflector was closed by a flat metallic disk with diameter D_B). The radiation patterns in the diagonal plane ($\phi = 45^\circ$) are depicted in Fig. 5. As expected, the gain of the shaped antenna (49.3 dBi) is higher than that of the classical configuration (47.8 dBi). The side-lobe levels of the shaped antenna are also higher (about 7 dB) than those of the classical configuration. One also observes a 4 dB increase of the cross-polarization peak of the shaped reflector antenna.

The shaping procedure of Section II is simpler and, consequently, faster than others based on the numerical integration of ordinary differential equations [2], [3]. To illustrate its numerical efficiency, we

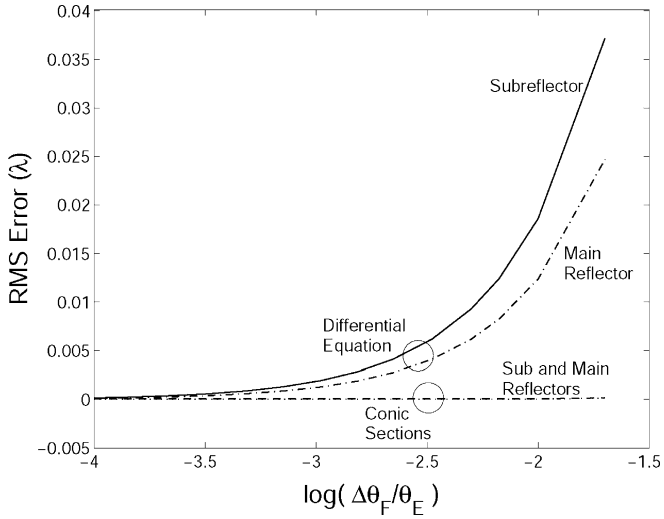

Fig. 6. RMS errors of the shaped ADC reflectors as functions of $\Delta\theta_F$.

present a comparison of surface error obtained by using different numbers ($N = \theta_E/\Delta\theta_F$) of synthesized points. As a reference, we employ a shaped dual reflector antenna synthesized with a large number of points ($N \approx 10^4$), as doubling it leads to differences of less than $10^{-5}\lambda$ between the surfaces. Fig. 6 presents the RMS error of the shaped reflector surfaces as function of $\log(1/N)$ for both schemes (i.e., the present procedure and another based on the numerical integration of a differential equation). Only points obtained at each step n were considered for the error calculation. For the subreflector the RMS error is calculated from the distances r_{Fn}, while for the main reflector the error is calculated from its coordinates z_n. The RMS error is actually dominated by the error at the reflector rims ($n = N$). From Fig. 6 one observes that the shaping procedure of Section II sustains very small RMS errors even for $\Delta\theta_F \approx \theta_E/50$ (i.e., with $N \approx 50$ conic sections used to obtain the points of each reflector generatrix). For the present ADC shaping, the formulation of [1] was also implemented and it has essentially the same convergence rate of the present formulation.

B. Shaped ADE Antenna

In the second case study, an ADE is shaped to provide a tapered aperture illumination. The antenna is similar to that investigated in [10], with $D_M = 40.64$ cm, $D_B = D_S = 6.6$ cm, $\ell_o = 21.08$ cm, and $\theta_E = 45^\circ$. For a classical ADE these parameters provide $V_S = 2.39$ cm [5]. The operating frequency is 14.7 GHz, such that $D_M \approx 20\ \lambda$. The feed model is still given by (27), but with $p = 23.5$ [10]. The tapered aperture illumination is described by

$$G_A(x) = 1 - \left(1 - E_M^2\right)\left(\frac{2x - D_B}{D_M - D_B}\right)^2 \tag{28}$$

where $D_B/2 \le x \le D_M/2$ and $E_M = 0.6$ [10]. The classical (dotted lines) and shaped (solid lines) ADE reflectors' generatrices are plotted in Fig. 7 together with the shaped subreflector caustic. The maximum deviation of the shaped reflectors with respect to the classical configuration is approximately 3 mm for both sub- and main-reflectors (see Fig. 7). The diagonal-plane radiation patterns of both classical and shaped antennas are illustrated in Fig. 8. Once again, for the MoM analysis, the main-reflector central hole was closed by a flat metallic disk. From Fig. 8 one observes that the tapered aperture illumination of (28) was able to slightly increase the antenna gain (from 34.4 dBi to

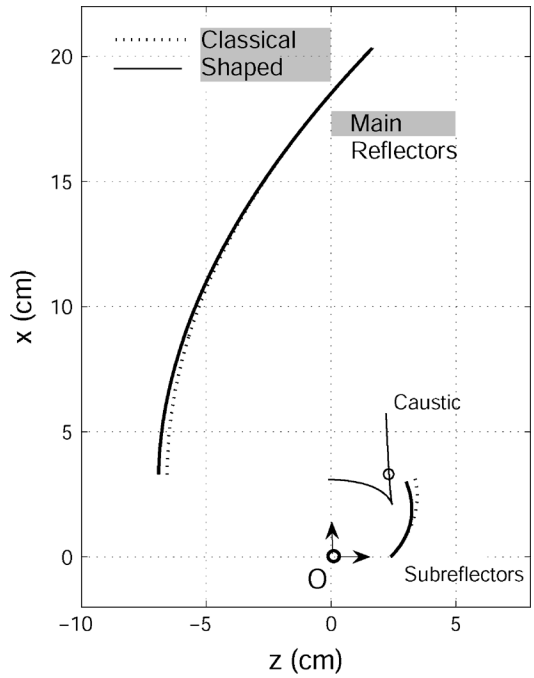

Fig. 7. Sub- and main-reflector generatrices of the classical (dotted lines) and shaped (solid lines) ADE antennas. The caustic refers to the shaped subreflector.

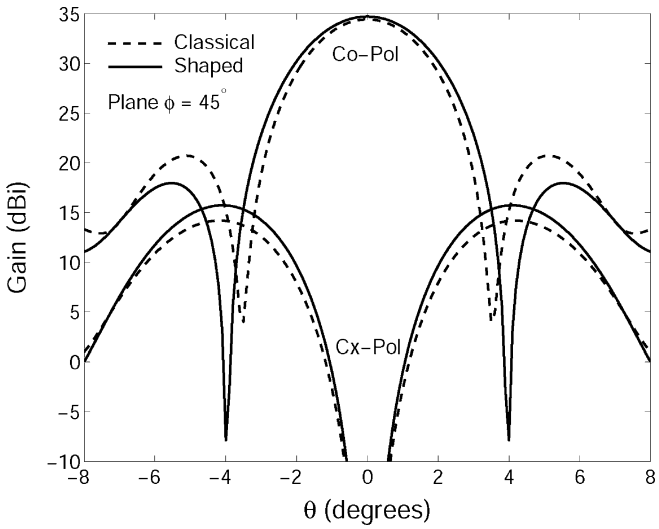

Fig. 8. Diagonal-plane radiation patterns of the classical (dashed lines) and shaped (solid lines) ADE antennas at 14.7 GHz. Reflectors shaped with $\Delta\theta_F \approx 10^{-4} \times \theta_E$.

34.7 dBi), with a small decrease of the first sidelobe level (about 1.5 dB) and a small increase of the cross-polarization peak (about 1.5 dB).

The convergence of the ADE shaping procedure is illustrated in Fig. 9. Its investigation was conducted similarly to the one previously performed for the ADC antenna and illustrated in Fig. 6. From Fig. 9 one observes that the shaping procedure of Sections II and III sustains very small RMS errors even for $\Delta\theta_F \approx \theta_E/10$ (i.e., with $N \approx 10$ conic sections used to obtain the points of each reflector generatrix).

V. Conclusion

A method for shaping axis-symmetric dual reflectors has been presented. The synthesis is based on the consecutive combination of local conic sections to represent the reflector's generatrices. The problem

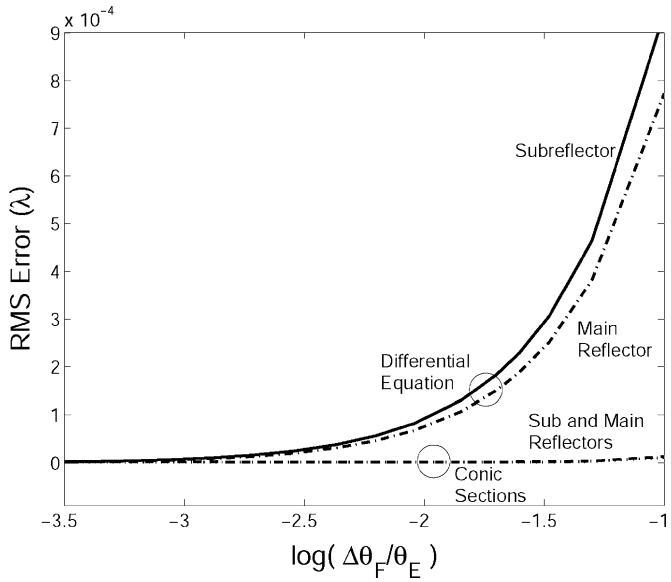

Fig. 9. RMS errors of the shaped ADE reflectors as functions of $\Delta\theta_F$.

was reduced to solving linear equations embedded in a stepwise numerical procedure. The procedure is valid for any axis-symmetric dual-reflector configuration with uniform phase distribution at the antenna aperture.

The shaping procedure has been successfully applied to the synthesis of a Cassegrain antenna with a uniform aperture illumination [1] and of an ADE configuration with a tapered aperture illumination [10]. All designs were further analyzed by a MoM technique for bodies of revolution to demonstrate the applicability of the shaping procedure, which is inherently based on GO concepts. The shaping procedure was also compared to another based on the numerical integration of an ordinary differential equation and it was verified that the former may converge with about 100 times less iterations.

References

[1] Y. Kim and T.-H. Lee, "Shaped circularly symmetric dual reflector antennas by combining local conventional dual reflector systems," *IEEE Trans. Antennas Propag.*, vol. 57, no. 1, pp. 47–56, Jan. 2009.

[2] V. Galindo, "Design of dual-reflector antennas with arbitrary phase and amplitude distributions," *IEEE Trans. Antennas Propag.*, vol. AP-12, no. 4, pp. 403–408, Jul. 1964.

[3] J. J. Lee, L. I. Parad, and R. S. Chu, "A shaped offset-fed dual-reflector antenna," *IEEE Trans. Antennas Propag.*, vol. AP-27, no. 2, pp. 165–171, Mar. 1979.

[4] P.-S. Kildal, "Synthesis of multireflector antennas by kinematic and dynamic ray tracing," *IEEE Trans. Antennas Propag.*, vol. 38, no. 10, pp. 1587–1599, Oct. 1990.

[5] F. J. S. Moreira and A. Prata, Jr., "Generalized classical axially symmetric dual-reflector antennas," *IEEE Trans. Antennas Propag.*, vol. 49, no. 4, pp. 547–554, Apr. 2001.

[6] A. Prata, Jr., F. J. S. Moreira, and L. R. Amaro, "Compact high-efficiency displaced-axis axially symmetric high-gain antenna for spacecraft communications," *JPL's IND Technol. Sci. News*, no. 17, pp. 9–14, May 2003.

[7] S. P. Morgan, "Some examples of generalized Cassegrainian and Gregorian antennas," *IEEE Trans. Antennas Propag.*, vol. AP-12, no. 6, pp. 685–691, Nov. 1964.

[8] B. S. Westcott, F. A. Stevens, and F. Brickell, "GO synthesis of offset dual reflectors," *IEE Proc.*, vol. 128, no. 1, pp. 11–18, Feb. 1981, Pt. H.

[9] J. R. Mautz and R. F. Harrington, An improved E-field solution for a conducting body of revolution Dept. Electrical and Computer Engineering, Syracuse University, Tech.Rep. TR-80-1, 1980.

[10] Y.-C. Chang and M. J. Im, "Synthesis and analysis of shaped ADE reflectors by ray tracing," in *IEEE Antennas Propag. Soc. Int. Symp.*, Jun. 1995, pp. 1182–1185.